ULTRA-LOW PHASE NOISE MICROWAVE EXTRACTION FROM MODE-LOCKED LASERS

by

Aram Kalaydzhyan

A Thesis Submitted in Partial Fulfillment
of the Requirements for the Degree of

MASTER OF SCIENCE (M.SC.)

in

PHYSICS

at the

UNIVERSITY OF HAMBURG

1st advisor: Prof. Dr. Franz X. KÄRTNER

2nd advisor: Dr. Ingmar HARTL

2014

Abstract

Ultra-low phase noise microwave extraction from mode-locked lasers.

This project was undertaken to design a balanced optical-microwave phase detector (BOMPD) for sub-femtosecond synchronization between optical and microwave sources. Those hybrid phase detectors form a constituent part of a large-scale synchronization system for future free-electron lasers (e.g. the European XFEL). The goal is achieved with 0.5 fs RMS jitter integrated from 1 Hz to 20 kHz. Furthermore, a microwave interferometric phase noise measurement system was created for high precision characterization of the synchronization system.

Erzeugung von Mikrowellen mit extrem niedrigem Phasenrauschen mittels modengekoppelter Laser.

Das Ziel dieser Arbeit war die Entwicklung von Phasendetektoren für die Synchronisation von ultrakurzen Laserpulsen und Mikrowellengeneratoren (BOMPD) mit einer Sub-Femtosekunden-Präzision. Der BOMPD ist ein wesentlicher Bestandteil des Synchronisationssystems für zukünftige Freie-Elektronen Laser wie z.B. der European XFEL. Die Synchronisation durch die BOMPD-Phasenregelschleife erzielte ein Jitter von 0,5 fs (quadratischer Mittelwert). Weiterhin wurde eine interferometrische Messaparatur zur hochpräzisen Charakterisierung des Phasenrauschens im Synchronisationssystem realisiert.

Erklärung zur Eigenständigkeit

Hiermit bestätige ich, dass die vorliegende Arbeit von mir selbständig verfasst wurde und ich keine anderen als die angegebenen Hilfsmittel – insbesondere keine im Quellenverzeichnis nicht benannten Internet-Quellen – benutzt habe und die Arbeit von mir vorher nicht einem anderen Prüfungsverfahren eingereicht wurde. Die eingereichte schriftliche Fassung entspricht der auf dem elektronischen Speichermedium. Ich bin damit einverstanden, dass die Masterarbeit veröffentlicht wird.

Contents

1 Inroduction **1**

1.1 Laser Frequency Comb . . . 1

1.2 Stabilization of an octave spanning Ti:Sapphire frequency comb . . . 2

1.3 Timing synchronization for large-scale facilities . . . 5

1.4 Laser to RF conversion . . . 6

2 Balanced Optical-Microwave Phase Detection **11**

2.1 Operation Principle . . . 11

2.2 Optical-RF hybrid PLL . . . 15

2.3 External noise sources . . . 18

2.4 Dual-frequency reference path . . . 19

3 Interferometric setup for phase noise measurements **21**

3.1 Setup scheme . . . 21

3.2 Measurement results . . . 22

4 Conclusion and outlook **25**

Acknowledgements **27**

A Ultra-stable microwave VCO **29**

B Low-noise amplifier **31**

C Calibration of the BOMPD setup **33**

References **33**

1 Inroduction

The main goal of the following Master's Thesis is to cover the subject of microwave generation from the laser frequency comb and to present the development of a balanced optical-microwave phase detector (BOMPD) for ultra-low jitter synchronization of a tunable microwave signal source to a femtosecond mode locked laser. Additionally, the setup with capabilities to measure the synchronization jitter of BOMPDs is presented.

1.1 Laser Frequency Comb

The Nobel Prize in Physics 2005 was shared by John Hall and Theodore Hänsch for the development of optical frequency comb technique [1] which had a direct impact in the fields of optical frequency metrology and optical clocks.

The first step in generation of optical frequency combs is locked in constructing of the periodic train of ultrashort pulses with high repetition rate, which is generated by a mode-locked laser. This pulse train has the frequency spectrum that consists of regularly spaced sharp lines. Such a frequency spectrum is, actually, an optical frequency comb. For exact prediction of the form of the frequency comb, let us first analyze a train of completely identical pulses with fixed repetition rate f_r. By usage of the Fourier transform one can see that this train generates a comb of regularly spaced Fourier transforms of pulse envelope functions, where the space is equal $1/f_r$ (see Fig. 1.1). If one measures such a spectrum with a resolution sufficient to differentiate the comb lines, one will not be able to differentiate the pulses in time. It will result in the positive interference of successive pulses inside the interferometer that occurs at nf_r, where n is integer.

Now we need to take into account the fact that the carrier envelope phase ϕ is not constant, but evolving with time. The phase shift from pulse to pulse $\Delta\phi = \phi_2 - \phi_1$ is constant and leads to a global offset f_0 of the whole frequency comb. The comb offset depends on phase shift as $f_0 = (1/2\pi)\Delta\phi f_r$. Thus the frequencies of the comb lines are $\nu_n = f_0 + nf_r$.

In an experiment the frequency nf_r could be measured in a straightforward way by counting pulses by a fast photodiode and dividing their number by the time of the measurement. The absolute measurement of the comb shift f_0 is more complicated and requires interferometric measurements. However, if the frequency comb spans an octave

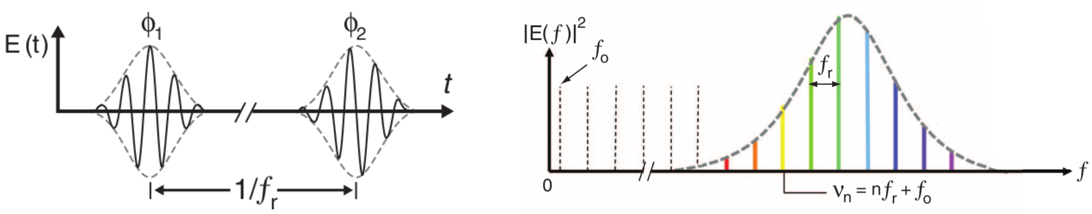

Figure 1.1: Time and frequency domain correspondence for a pulse train with evolving carrier-envelope function; *(left)* Time Domain, *(right)* Frequency Domain [2].

in frequency (i.e., the highest frequencies of the comb are a factor of two larger than the lowest frequencies), measurement of f_0 is significantly simplified. In this case one can use second harmonic crystal for doubling of a low frequency comb line and analyze its interference with the high frequency comb line of about doubled frequency. Thus, if one stabilizes both the repetition rate f_r and the carrier-envelope offset frequency f_0 of a laser frequency comb, it will be possible to control positions of the comb lines extremely precise.

1.2 Stabilization of an octave spanning Ti:Sapphire frequency comb

Since it is possible to generate an octave spanning spectra directly from a Ti:sapphire laser [3], this class of mode-locked lasers became very attractive as a base for ultra-stable laser frequency comb generation. Suppose, we have one with a configuration shown in Figure 1.2.

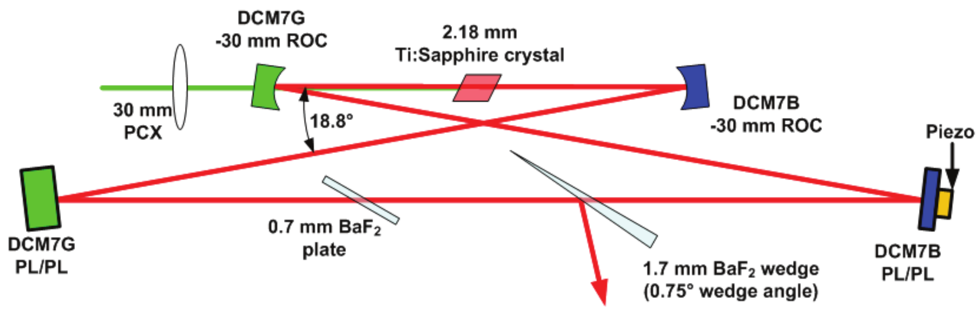

Figure 1.2: Example schematic of an octave Spanning Ti:Sapphire laser. The length of the ring cavity could be slightly corrected by moving of the DCM7B flat mirror with a piezo attached on the back side of it [4].

In this scheme a ring configuration of the mode-locked laser is presented. The cavity is built from two curved and two flat mirrors. One of the curved mirrors is semi-transparent and the system is pumped by a CW laser through it. One of the flat mirrors could be slightly moved by driving the piezoelectric transducer crystal. The Ti:Sapphire crystal works as an active media, while the BaF_2 plate compensates group delay dispersion of the light pulses in mirrors, Ti:Sapphire and air. The BaF_2 wedge is a double-purpose element: first, it is used for fine tuning of dispersion correction, second, it plays a role of the output coupler.

Two degrees of freedom associated with the optical comb, the laser repetition frequency f_r and the carrier-envelope offset frequency f_0, can be presented as

$$\begin{aligned} f_r =& \frac{v_g(f_c)}{l_c}, \\ f_0 =& f_c\left(1 - \frac{v_g(f_c)}{v_p(f_c)}\right), \end{aligned} \tag{1.1}$$

where l_c is round-trip cavity length, v_g and v_p are, respectively, the average group and phase velocities inside the cavity and f_c is the spectrally weighted carrier frequency. To control two degrees of freedom, it is required to drive at least two of presented parameters. One of them, the cavity length l_c, could be changed directly by moving the flat mirror with use of the piezo transducer. A possibility to fix the second degree of freedom comes from the fact that the carrier frequency f_c shifts as a function of the intracavity pulse energy, and, therefore, it can be driven by modulation of pump power [5, 6]. Variation of the pump power can be done, for example, with use of an acousto-optic modulator (AOM). Thus, the feedback system is complete and it possible to lock the carrier frequency to zero with the self-referencing technique and, after that, lock one comb tooth to a reference oscillator frequency, for example, hydrogen maser standard or stable CW laser (Fig. 1.3, left).

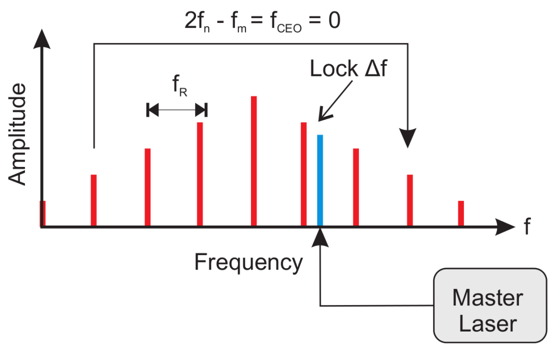

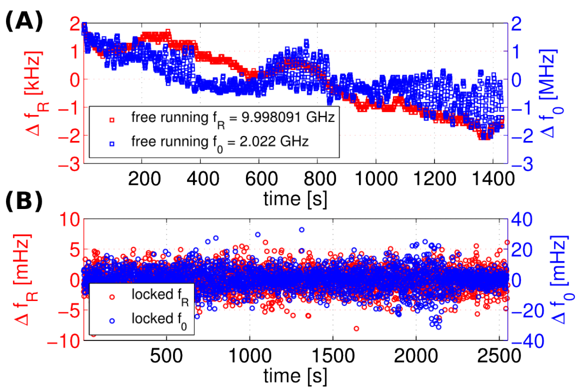

Figure 1.3: **Left:** Stabilization scheme of an octave spanning laser comb in the frequency domain. The carrier envelope frequency is locked to zero by referencing one tooth of the laser comb to a second one of the lower frequency, which frequency is doubled. Repetition rate of the comb is controlled by referencing of one of comb lines to a reference frequency standard. **Right:** Counting record of the offset frequency and the repetition rate for the Ti:sapphire laser [7] in the free running mode *(A)* and after locking *(B)*.

A similar technique was already applied to stabilize the laser-based optical frequency comb with a 10-gigahertz repetition rate, whose output spectrum covers the range from 470 to 1130 nanometers (i.e. over one octave) [7]. Figure 1.3 (right, a) shows the long term drifts of carrier-envelope offset frequency f_0 and the laser repetition rate f_R while all phase-locked feedback loops are off. Easy to see that both frequencies show a large drift. It is notable, that the the drift of the offset frequency f_0 is more than three orders of magnitude larger than the drift of the repetition rate f_R. After the stabilization system is activated, both frequencies stay within tens of mHz. These drifts correspond to the fractional instability provided by the hydrogen maser and the synthesizers, which means that the noise characteristics of the laser itself might be even better. Obtained phase noise performance of the stabilized laser is presented in Figure 1.4. Integrated phase jitter of the generated pulse train is about 0.3 rad from 10 Hz to 10 kHz, referred to 10 GHz carrier. Sharp peaks of the noise performance curve in the region around 10 kHz correspond to the operating bandwidth of the f_0-PLL. Other peaks at higher frequencies have thermal and electronic origins. These factors increase the full integrated phase noise which is about 3 radians from 10 Hz to 1 MHz.

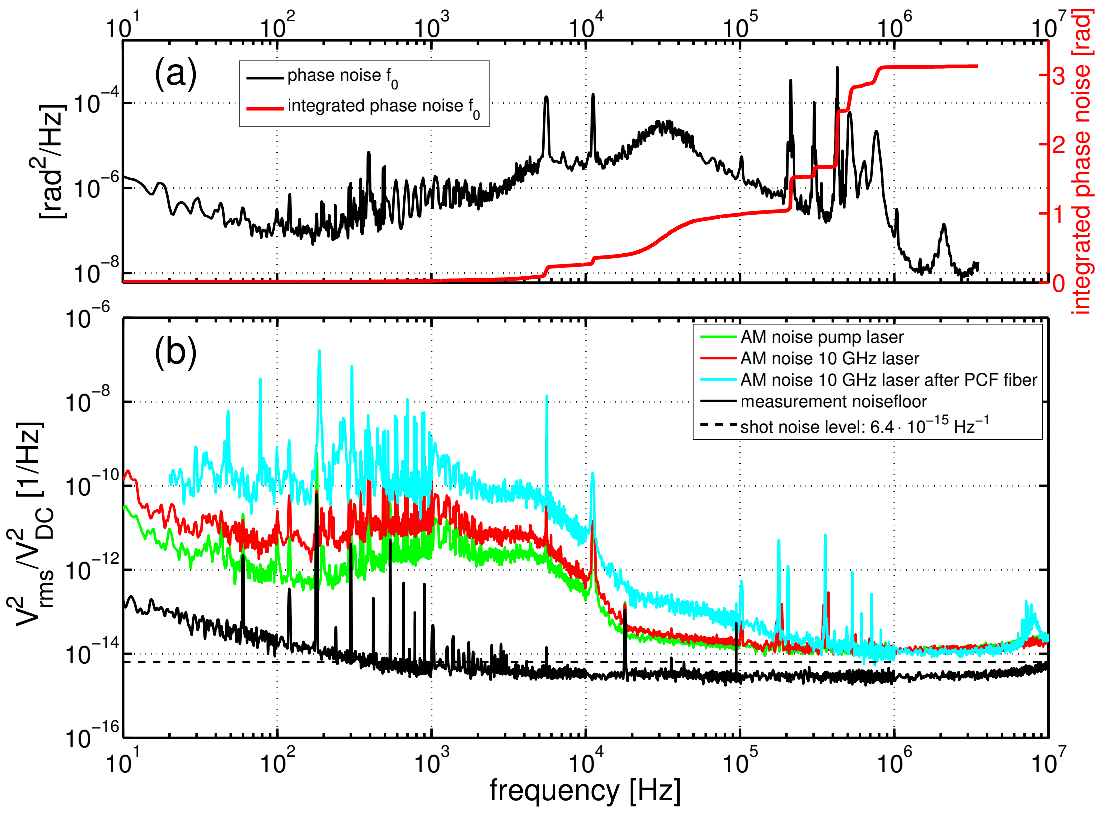

Figure 1.4: **(a)** Carrier envelope frequency phase noise and integrated phase noise. **(b)** Amplitude noise characteristics of the pump laser and the 10GHz laser [7].

1.3 Timing synchronization for large-scale facilities

As shown, a drift-free high frequency pulse train can be generated from the femtosecond mode-locked laser, which means that it can be used as a master clock source for various scientific experiments. However, the fact that the clocking signals are presented in the form of ultra-short laser pulses stands it out against other types of clocking sources and RF-signal distribution systems. These femtosecond pulses could be transported over large kilometer-scale distances directly through optical fiber links. The laser optical clock is very proper solution for timing synchronization between different parts of large-scale scientific facilities, such as particle accelerators and X-Ray free electron lasers (FELs). One of the FELs, the European XFEL, requires the tight synchronization between many optical sources (such as high power laser for the electron gun, seeding laser, laser for pump-probe experiments etc.) and microwave devices (such as pulsed clystron, accelerating modules, bunch compressors, beam diagnostics tools and others). A proper configuration for distribution of the timing signal was proposed more than ten years ago in the framework of the, so called, MIT Bates X-ray laser project [8].

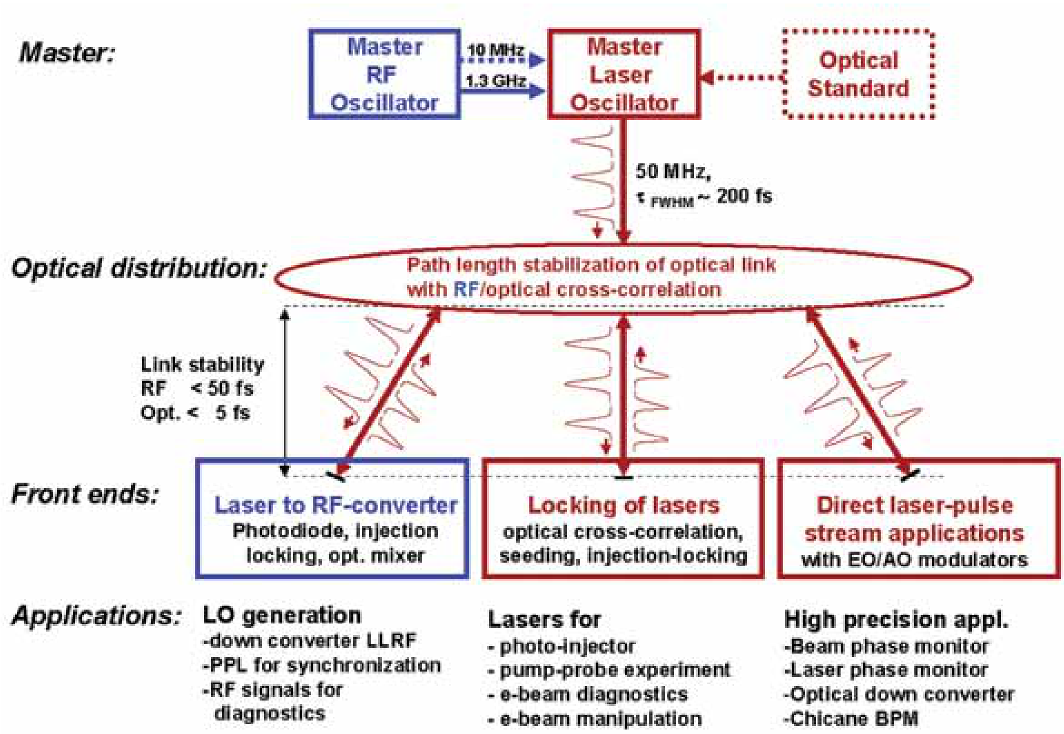

Figure 1.5: Multilevel scheme of the laser-based synchronization system for the XFEL. First level: Master Laser Oscillator generating a periodic stable stream of identical optical pulses. Second level: The length-stabilized fiber-link distribution system. Third level: application-dependent front-ends.

This scheme was adapted for the configuration of the European XFEL (see Fig. 1.5), where all sub-systems of the FEL are referenced with a master-laser oscillator (MLO) which is locked to a low-noise RF oscillator or to an optical frequency standard. The MLO is producing a train of ultra-short optical pulses centerd at a wavelength of 1550 nm [9]. This pulse train is transported to the subsystems of the FEL through optical fiber link with stabilization system that maintain constant the round trip time for pulses propagating in a fiber link with a feedback loop that changes its length [10]. After the optical pulses are delivered to the end-stations or subsystems of the FEL, they will be either directly used in high-accuracy direct timing measurements, or used for optical-to-optical synchronization of other laser laser systems of the facility, or be converted to radio frequency (RF) signals for referencing of accelerating modules. Issues of the optical-to-RF synchronization are the main subject of the thesis.

1.4 Laser to RF conversion

Direct detection

The European XFEL's timing distribution system is required, in particular, to provide high-frequency RF signal referenced to the optical signal with sufficient output power and femtosecond stability. A straightforward approach to extract RF signal from optical frequency comb is to detect the optical signal with a fast photodiode, and then filter out the required frequency comb line with a suitable band-pass filter (see Fig. 1.6). Afterwards the generated weak RF signal needs to be amplified to the required power level.

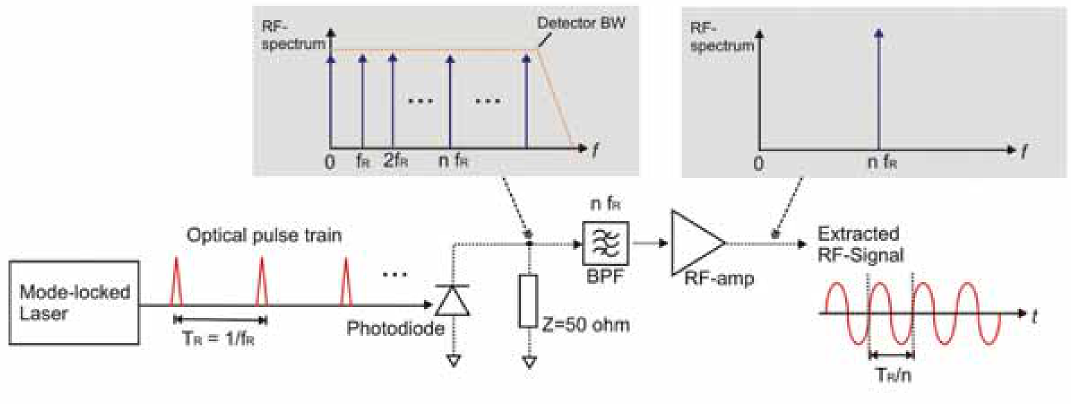

Figure 1.6: Scheme of the microwave signal extraction from an optical frequency comb via direct detection with fast photodiode.

Since fast GaAs and InGaAs photodetectors with a bandwidth over than 10 GHz appeared on the market, they became the most cost-efficient solution for many applications in microwave extraction experiments [11]. However, there are some performance limitations mainly caused by the effects listed below.

The photodiodes utilize the photovoltaic effect to convert optcal power into an electrical current. This current flows through the load resistor across which the output voltage of the photodetector is measured. The thermal noise of the load resistor makes the largest contribution into the limitation for the measurement of phase noise at high offset frequencies. To increase the signal-to-noise ratio one should put as much optical power to the photodetector as possible while it is not saturated.

Photodiodes have the internal capacitance created by PIN junction. This capacitance depends on the design of PIN junction and spatial charge distribution in the photodiode. It leads to the appearance of the nonlinear process of the hence the phase of the output signal (see Fig. 1.7) which is the origin of the amplitude-to-phase (AM-PM) conversion process in the photodiode. The AM-PM conversion factor usually varies between 1 and 10 ps/mW, depending on the type and size of the photodiode. It means that if we apply a maximum power of 10 mW on a photodiode with the AM-PM conversion factor of 1 ps/mW, then we will have to control the applied optical power within 0.1% to reach at least 10-fs jitter level (or 0.01% for 1-fs jitter), while all other phase noise sources are not taken into account. Such requirement it already a very complicated issue to solve.

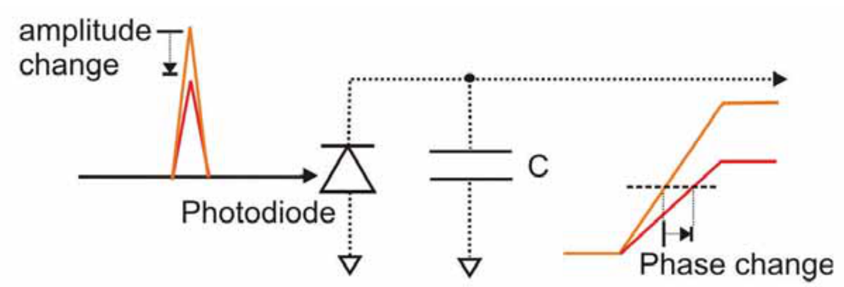

Figure 1.7: AM-to-PM conversion through direct detection of an optical pulse with fast photodiodes. Due to internal non-zero capacitance of photodiodes the rise time of the electrical signal generated by the incoming laser pulse depends on the energy of the pulse. Therefore, amplitude noise in the optical domain converts to phase noise in the electronic domain.

Finally, the response of the photodetector depends on temperature which has a direct impact on very slow phase drifts of the timing signal. Additionally to that, changes of the room temperature may cause mechanical deformation of the setup and slight optical misalignment. Temperature stabilization of 0.1°C does not eliminate a high degree of correlation between the photodiode temperature and the phase jitter [12]. To summarize, the direct detection scheme requires a deep improvement of detector designs in directions of increasing of saturation power and suppressing of the AM-PM conversion. There are already the designs that make a phase jitter below 10fs achievable [13, 14], but for the time present are difficult for real implementations.

Hybrid locking of low noise RF oscillators

Alternative technique of the optical to RF conversion deviates from direct generation of microwave signals from laser pulses, but uses the pulse train for the phase referencing of a local RF oscillator to regenerate an ultra-low noise RF signal. This approach is well-founded since ulta-low phase noise voltage control oscillators (VCOs) are available on the market. These VCOs generate RF signals of microwave frequencies (1 GHz - 12 GHz) and could be tuned only in few kHz for the whole feedback voltage range. A 10.8 GHz commercial sapphire-loaded cavity oscillator (SLCO) was used as a VCO during the work on the Thesis (see Appendix A). This VCO generates +12 dBm power signal with the single sideband phase noise curve shown in Figure 1.8. The phase noize curve settles below -150 dBc\Hz level by offset frequency over 10 kHz which results in only about 0.3 fs jitter integrated from 1 kHz to 10 MHz [15]. This low noise performance is achieved by locking of the VCO to a thermally and acoustically stabilized cavity inside the SLCO. However, the phase curve rises rapidly by decreasing of the offset frequency. The only integrated jitter from 100 Hz to 1 kHz adds 2 fs more to the total RMS jitter of the signal source. This behavior inevitably results in phase drifts during long-term operation.

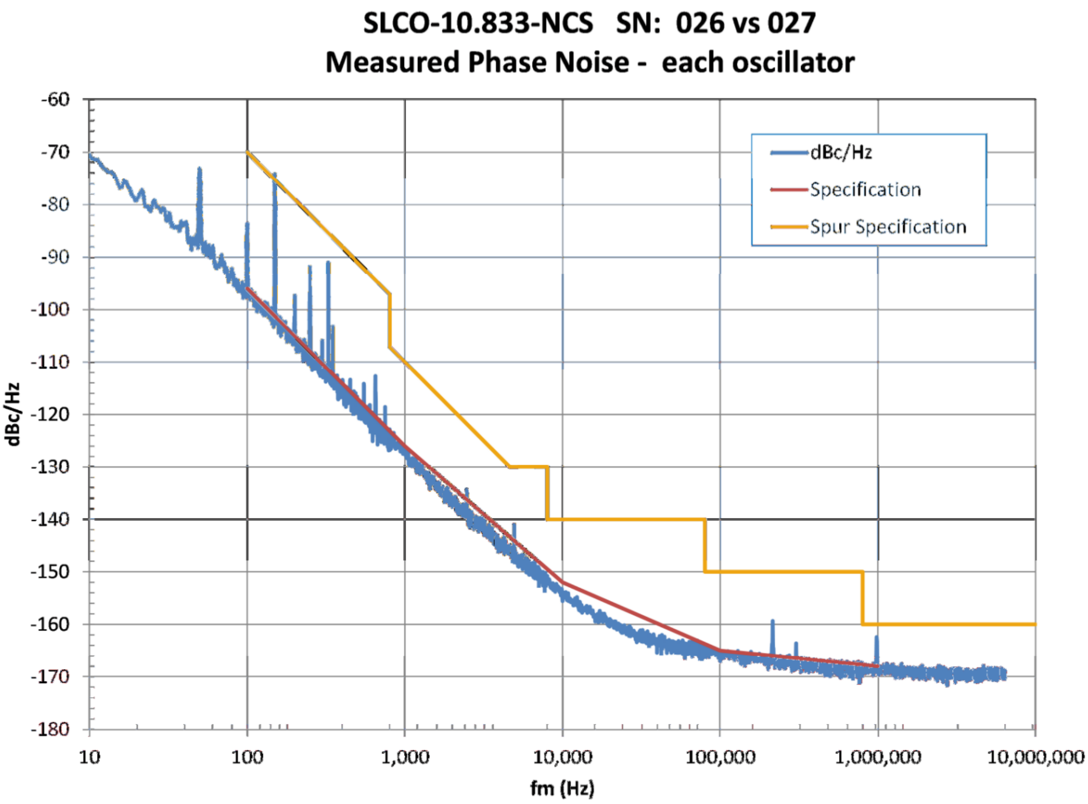

Figure 1.8: Variation of the single-sideband (SSB) phase noise of free-running SLCOs at 10.833 GHz carrier frequency with offset from carrier frequency.

On this account, even low-noise RF sources need to be referenced to a timing distribution system. Thereto one can build a phase-locked loop (PLL) which scheme is shown in Figure 1.9. There is a locally staying VCO which RF output signal is used in subsequent experiments. The same signal is fed to a hybrid optical-RF detector which is sensitive to the phase error between this RF signal and incoming optical reference pulses of the laser-based synchronization system. The PLL is accomplished by a loop filter (for example, PID controller) which is tuning the VCO according to the detected phase error.

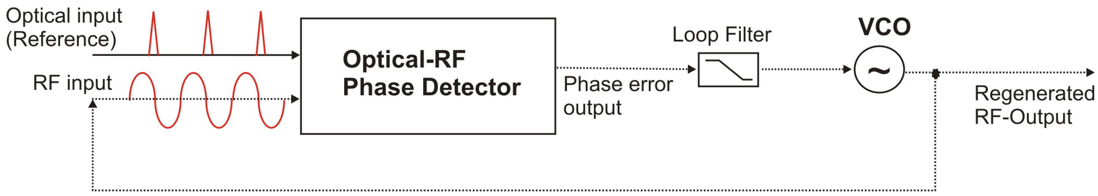

Figure 1.9: Schematic diagram of a opto-electronic phase-locked loop.

Since the maximum response frequency of loop filters is limited, the presented scheme will combine the advantages of VCO's low phase noise characteristics at high offset frequencies and drift-free performance of the laser oscillator. But it is a challenging task to design a high-responsive optical-RF phase detector which would be not sensitive to power and temperature drifts. One of developed hybrid phase detectors, balanced optical-microwave phase detector or BOMPD, is discussed in the next chapter.

2 | Balanced Optical-Microwave Phase Detection

2.1 Operation Principle

The AM-PM conversion by the optical-RF synchronization could be significantly reduced by use of balanced detection technique [16], where the phase offset measurement between RF and laser pulses is moved to the optical domain. The general concept is shown in Figure 2.1.

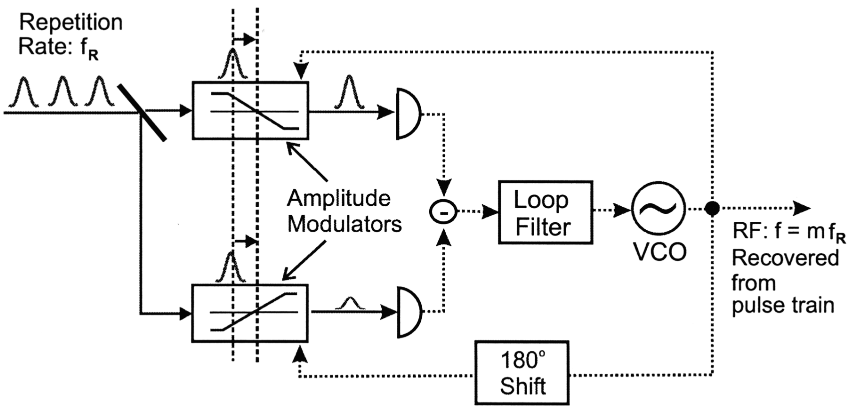

Figure 2.1: General scheme for microwave signal extraction an optical pulse train by transferring phase offset information into the optical domain.

The power of the incoming optical pulse train is equally divided and guided in two arms with amplitude modulators. These amplitude modulators driven by the same RF signal generated by the VCO, however the phase of the one them is shifted by 180°. Optical signals generated in two arms are detected by a balanced detector. This intensity difference depends on the phase offset between optical and RF signal and is equal to zero only when pulses of the optical pulses are coming to the amplitude modulators simultaneously with zero-crossings of the RF signal. Any phase misalignment from this position will produce a non-zero signal in the output of the balanced detector proportionally to the phase difference. This is a sufficient condition for a loop filter operation, which will tune the VCO to follow the phase of the reference laser pulse train.

Thus, this hybrid detection scheme is not sensitive to the amplitude of incoming laser pulses and will block AM-PM conversion if the PLL maintains phase equilibrium state. However, strict stability requirements are applied to the optical part of the phase detector. Thermal drifts and mechanical vibrations of the optical components will directly led to unbalancing of the detector and insertion of excessive phase noise to operation of the VCO. For example, especially for this reason, hybrid phase detectors based on a Mach-Zehnder interferometer cannot perform sub-10-fs stability [17].

Such effects are significantly reduced by using of a fiber Sagnac-loop, which is constructed by a 50/50 fiber coupler where the ports on one side are connected to each other and two remaining ports are used as the input and output ports. The coupler is designed in the way to provide 50% power coupling between the fused fibers, so each laser pulse is divided into two equal pulses propagating through the fiber loop in opposite directions and meet again in the coupler. Interfered signal is guided toward the output (see Fig. 2.2, *left*).

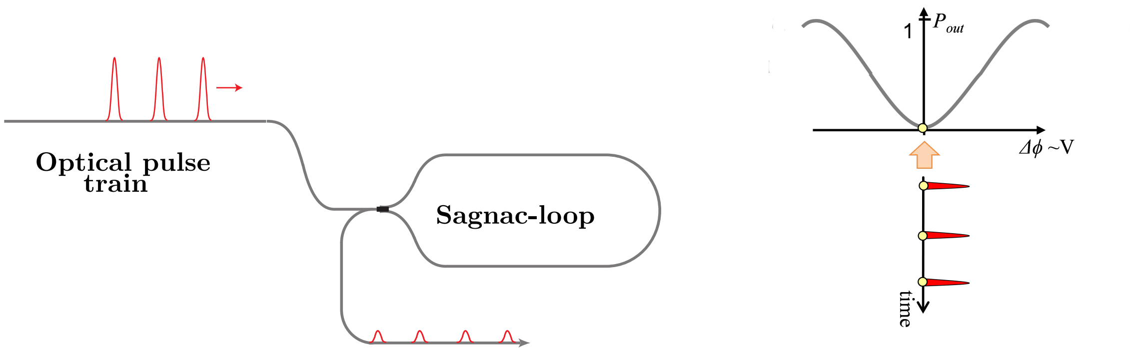

Figure 2.2: *(left)*: Scheme of the primitive fiber Sagnac interferometer. *(right)*: The phase between interfered pulses is absent and the output signal amplitude is equal zero according to the Sagnac-loop transmission function (2.2).

Since the CW and CCW propagating pulses run the same fiber length, a perfect destructive interference occurs in the output of the Sagnac-loop. The CW and CCW propagating paths are the two arms of the balanced detection scheme shown in Figure 2.1, which cannot be detuned by temperature or power drifts.

Suppose that the optical pulses are very short, we can describe the optical pulse train applied to the Sagnac-loop as a sequence of delta-functions:

$$P_{in}(t) = P_{in}^{avg} \frac{1}{f_R} \sum_{n=-\infty}^{\infty} \delta(t - \frac{n}{f_R}), \tag{2.1}$$

where P_{in}^{avg} is the average amplitude of the pulse train and f_R is its repetition rate. The output amplitude is given as

$$P_{out} = P_{in}\,\sin^2(\Delta\theta/2), \tag{2.2}$$

where $\Delta\theta$ is the phase shift between the CW and CCW propagating pulses and is equal zero in case of a simple Sagnac-interferometer (see Fig. 2.2, *right*). If one will implement a phase modulator into the Sagnac-loop and will drive it with regenerated repetition frequency divided by two (see Fig. 2.3, *left*), then the intensity of outgoing pulses is not equal zero:

$$P_{out} = P_{in}\,\sin^2\Big(\Phi_m\,\sin(\pi f_R t + \Delta\phi)\Big), \tag{2.3}$$

where Φ_m is the amplitude of phase modulation by $f_R/2$ frequency and $\Delta\phi$ is its phase relative to the pulse train. As one ca see, if the phase $\Delta\phi = \pi/2$ then every odd and even optical pulses in the train are modulated with the same signal amplitude, but with phases shifted by 180 ° (see Fig. 2.3, *right*). Results of interference for odd and even pulses are indistinguishable and the build a train of identical pulses with repetition rate f_R. Reference signal $f_R/2$ is driving

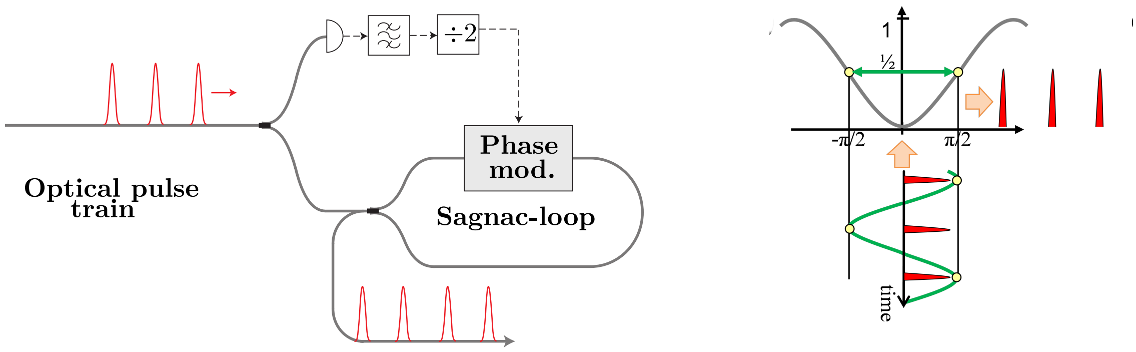

Figure 2.3: *(left)*: Reference signal $f_R/2$ is driving the phase modulator cut into the Sagnac-loop. *(right)*: Synchronized electro-optical sampling of the pulses with 180° phase shift results in generation of the train of equal pulses.

Finally, we supplement the scheme with the RF signal source with a frequency equal to a multiple of repetition rate, $f_0 = N f_r$, which we want to lock to the optical reference signal (see Fig. 2.4, *left*). We add the signal from the VCO to the modulation signal:

$$P_{out} = P_{in}\,\sin^2\Big(\Phi_m\,\sin(\pi f_R t + \pi/2) + \frac{\Phi_0}{2}\,\sin(2\pi f_0 t + \Delta\theta)\Big), \tag{2.4}$$

where Φ_0 is the amplitude of phase modulation from the VCO and $\Delta\theta$ is the phase error between the laser pulse train and the VCO signal. By substituting of (2.4) to (2.1) the master equation for the output signal function is deduced,

$$P_{out} = P_{in}^{avg} \frac{1}{f_R} \sum_{n=-\infty}^{\infty} \sin^2\Big(\Phi_m \sin(\pi f_R t + \pi/2) + \frac{\Phi_0}{2}\sin(2\pi f_0 t + \Delta\theta)\Big)\ \delta(t - \frac{n}{f_R}), \quad (2.5)$$

which qualitatively means that the odd and even outgoing pulses have different amplitudes when the phase error $\Delta\theta$ is not equal zero. Periodic leaps of the generated pulse train could be interpreted as a modulation of the signal with the frequency $f_R/2$. Amplitude of the spectral component could be extracted from (2.6) for the small values of the phase error $\Delta\theta$ [17]:

$$P_{out}^{f_R/2} = 2P_{in}^{avg}\ \Phi_m \Phi_0 \Delta\theta. \quad (2.6)$$

The derived equation shows that the $f_R/2$ component of the signal which is coming out from the Sagnac-loop is linearly dependent on the phase error between the signal of the RF-oscillator and the optical clock. One can make a conclusion, that with proper detection, filtering and downsampling of that component the shown scheme functions as a hybrid optical-RF phase detector.

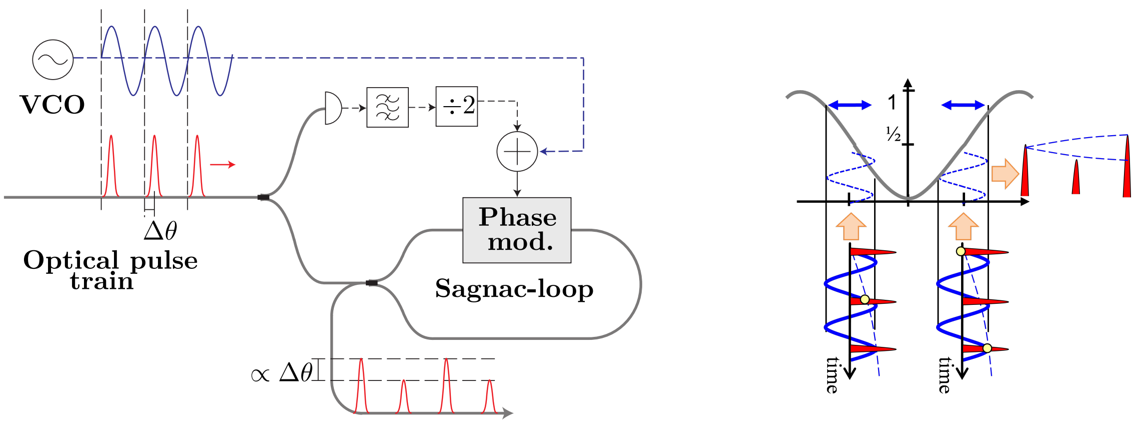

Figure 2.4: *(left)*: Scheme of the BOMPD sensitive to the phase error $\Delta\theta$ between RF-signal and referencing optical signal. *(right)*: VCO signal additionally applied to the phase detector causes amplitude modulation of output signals proportionally to $\Delta\theta$.

2.2 Optical-RF hybrid PLL

Basic scheme of the measurement setup

A standard experimental setup for the referencing of a VCO to the optical timing signal using a BOMPD is shown in Figure 2.5. The same scheme was taken as a base for one of the performed experiments with BOMPD. In this experiment a commercial (OneFive, Origami) free-running femtosecond Er-doped mode-locked laser manufactured was generating the input pulse train centered at 1558 nm with a 216.667-MHz fundamental repetition rate. The optical power is split into Sagnac-loop interferometer and, so called, reference path, where the 0 dBm signal is detected with a high speed InGaAs PIN photodiode (Discovery; DSC40S). After that, in the reference path, the 12.78 GHz harmonic is extracted from the pulse train with use of a narrow band-pass filter and divided by 2 in the frequency divider (Hittite; HMC492LP3). Cascades of various low-noise and power RF amplifiers (Hittite, Ciao Wireless) are used for maintaining of the RF signal on required power level. Derived 6.39 GHz signal is afterwards added in the diplexer (K& L) to 10.833 GHz signal generated by the SLCO. This signal, finally, drives the phase modulator implemented to the Sagnac-loop (EOSpace). Important to note, that variable phase shifters (ARRA) are required for setting of the relative phase offset between the RF modulating signal and optical train in the Sagnac-loop to $\pi/2$ (quadrature bias). The modulated pulse train at the output of the Sagnac-interferometer is detected on the photodiode with 15GHz detection bandwidth (EOT; ET-3500F) and down-sampled with 6.39 GHz signal from the reference path by proper in-phase tuning (ARRA), mixing (Mini-Circuits) and filtering the frequency components below 22 MHz with the low-pass filter (Mini-Circuits). This scheme in essence constructs the hybrid phase detector.

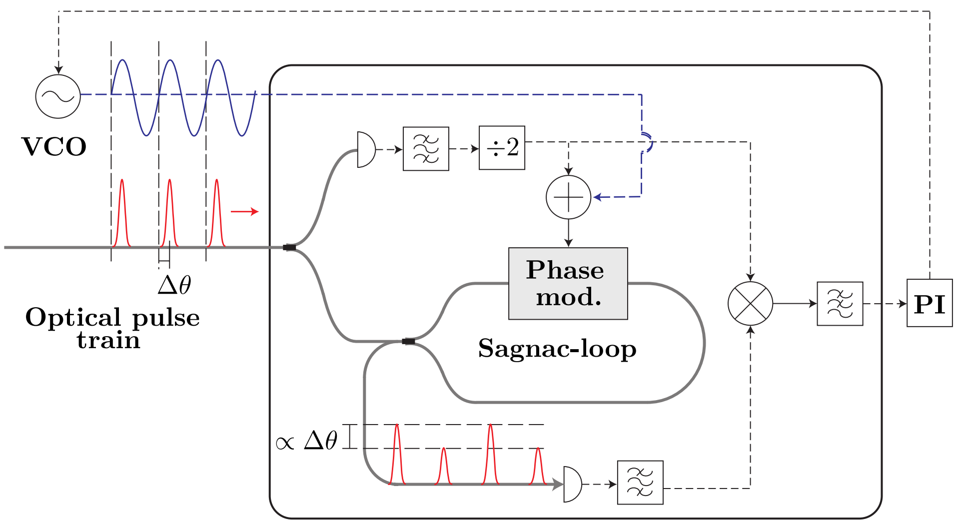

Figure 2.5: Scheme of the Optical-RF hybrid PLL based on BOMPD (in the frame).

Sensitivity of the constructed BOMPD is 6.0 mV/fs referred to 10.833 GHz (for the description of phase sensitivity measurement see Appendix C), which is sufficient for direct driving of a proportional-integral (PI) controller (Vescent; D2-125). The PI controller tunes the VCO frequency according to the error signal with maximum locking bandwidth of 100 kHz and performs a long-term stable lock between the mode-locked laser and the VCO.

For performing of both in-loop and out-of-loop PLL phase noise characterization the second almost identical BOMPD was built. This second BOMPD with phase sensitivity of 5.2 mV/fs referred to 10.833 GHz is not taking part in phase locking and is only required for characterization of the PLL performance (see Fig. 2.6).

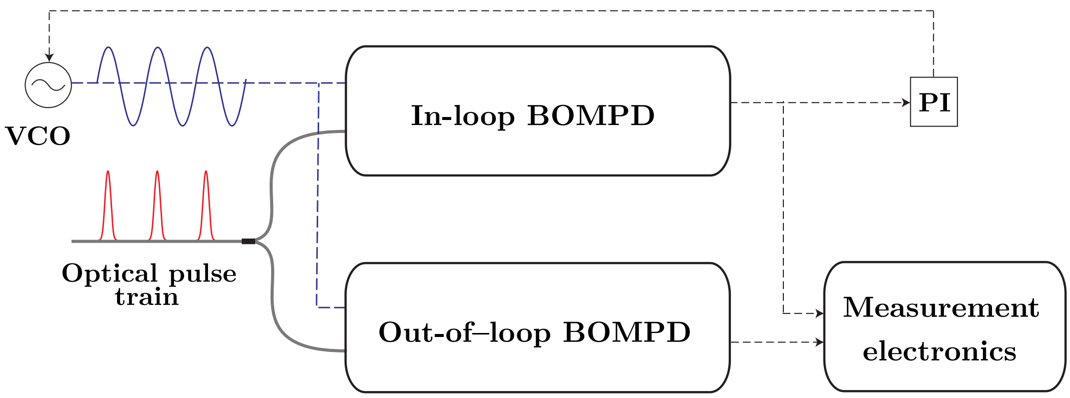

Figure 2.6: Scheme of the setup with two BOMPDs for in-loop and out-of-loop measurements of the PLL phase noise performance.

Output signals from both BOMPDs were measured with the signal source analyzer (Agilent; E5052B) and afterward converted to phase noise spectra with use of measured phase sensitivity coefficients. Signal amplitude level at BOMPDs' outputs is lower than the measurement noise floor of the SSA, therefore a low-noise preamplifier was used to increase the power level by 40 dBm (see Appendix B). Additionally, the phase noise performance of the mode-locked laser and microwave sources was measured by direct detection of the optical train and mixing of the output signals of two loosely locked SLCOs, respectively. It was investigated that the fiber-based laser produces the optical pulse train with higher phase jitter than new stable SLCOs. Therefore, it was decided to switch the setup to the optical-to-RF locking mode to make a deeper analysis of limits of BOMPD performance. In this mode VCOs frequencies loosely locked and the PLL is tuning the MLL repetition rate by driving the piezo transducer inside the laser. This locking mode is required for referencing of the laser master clock to a local ultra-stable RF frequency standard source.

As would be expected, variation of the parameters of the loop filter has a direct impact on the PLL performance. Gain of the PI-controller should maximized for the best phase noise suppression. However, if the loop filter gain will be too high, self-exciting oscillations of the loop appear or the PLL lose the lock completely. Thus, while tuning of phase loop parameters one should find the highest gain when the PLL keeps long-term stability. Residual phase error measurement curves for tight locking are shown in Fig. 2.7. The bandwidth of the PLL was limited to 20 kHz to avoid excitation of a resonant peak at 30 kHz. Signals measured at outputs of in-loop and out-of-loop BOMPDs are shown in blue and red, respectively. The integrates out-of-loop jitter is 0.5 fs for the whole locking bandwidth from 1 Hz to 20 kHz. Additionally, in-loop photodetection noise floor is shown in green. As one can see, performance of the phase lock is fundamentally limited to this noise floor. Increase of the noise curve close to 20 kHz correspond to operation of the loop filter. Various sharp peaks are excited by several environmental noise disturbers which are discussed below.

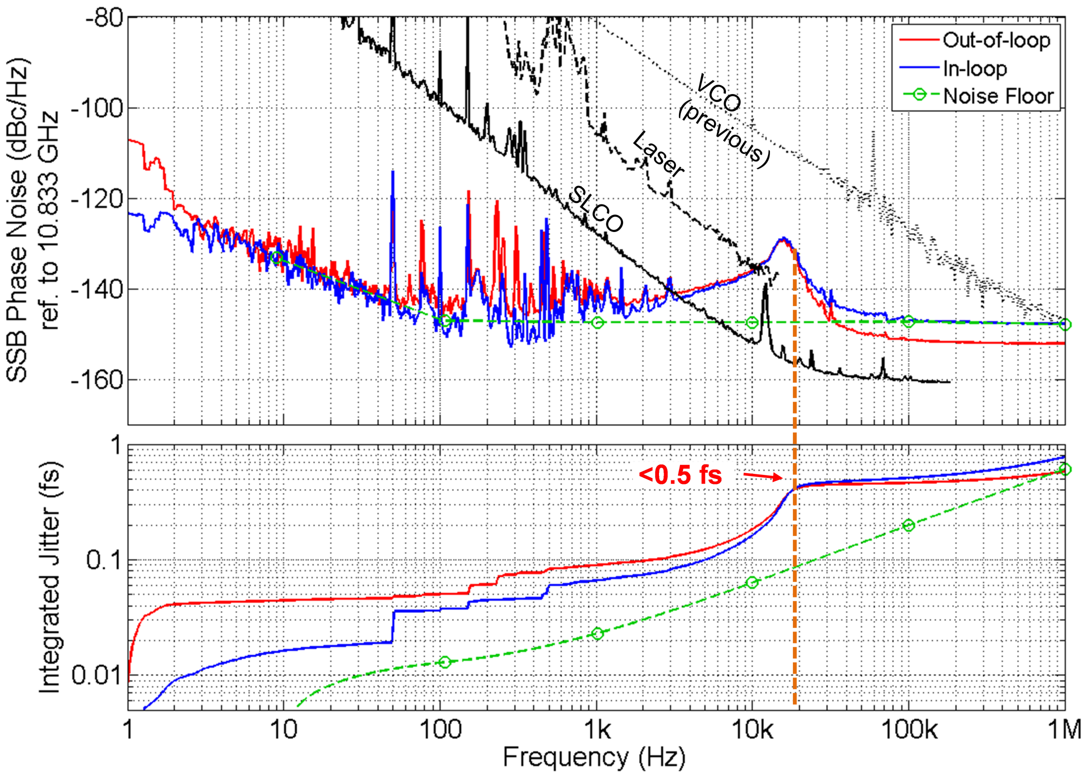

Figure 2.7: Single-sideband (SSB) phase noise spectra at 10.833 GHz and integrated jitter of the in-loop and out-of-loop PLL measurement (*blue* and *red*, respectively), in-loop photodetection noise floor (*green*), free-running SLCO (*solid black*) and laser (*dashed black*).

2.3 External noise sources

During adjustments of the BOMPDs for optimal operating it was found that the BOMPD phase noise performance is very sensitive for the electrical noise generated by surrounding equipment. A direct way for the penetration of external noise is the power supplying of various RF-electronics of the BOMPD. In Fig. 2.8 one can see the RF-noise generated by a typical switched mode power supply was measured by capturing of the AC signal spectrum by the SSA on the passive load supplied by DC current. Large spikes at 50 Hz, 100 Hz and 150 Hz are induced by transformers that work on 50Hz frequency of the standard 220 V AC power network. Various peaks below 1 kHz originate in the operation principle of switched mode power supply where broadband noise is created by under-damped oscillations in the switching circuit. Power supplies with high-degree output noise suppression are used to avoid undesirable noise excitation. Variation of the supplying voltage for different RF-components is managed using low-dropout (LDO) regulators. They also suppress low-frequency AC oscillations induced in long powering wires.

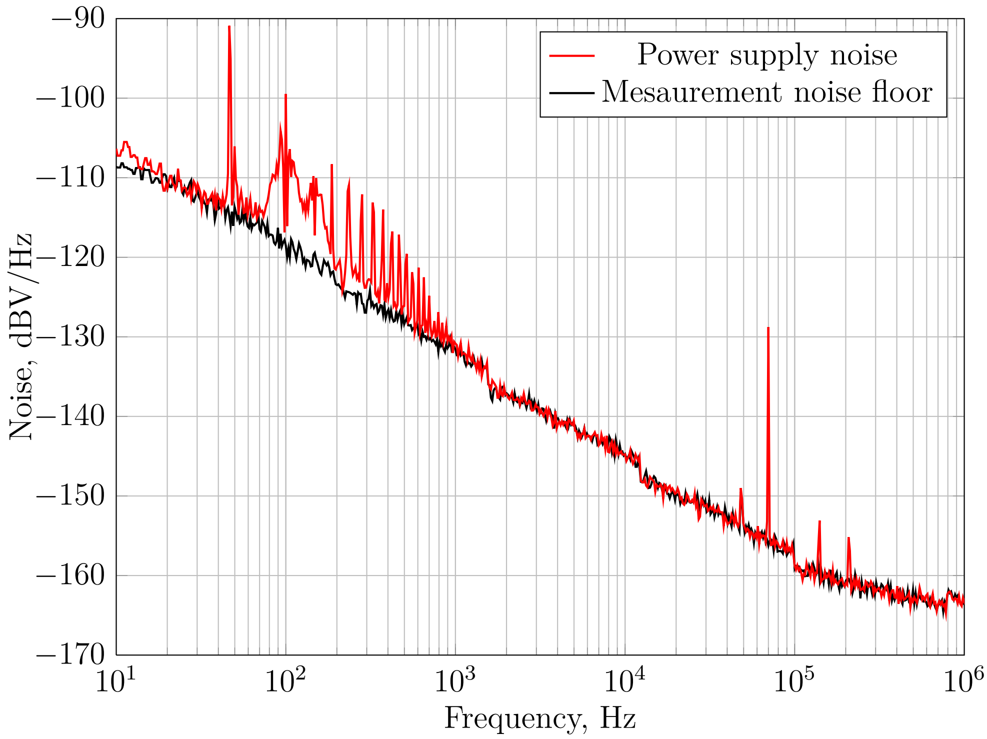

Figure 2.8: Noise spectrum of a 12 V switching mode power supply. Measured with 1/100 gain.

Sharp high-frequency peaks around 100 kHz correspond to the clocking frequencies of the digital signal processing system of the measurement electronics. Therefore, all signals are routed through wide bandwidth RF transformers before they are measured by laboratory equipment such as a spectrum analyzer or an oscilloscope.

The same noise is also radiated in the form of electromagnetic waves and detected by ground loops of the setup or direct pick-up from air. This electromagnetic interference (EMI) is minimized by sufficient distancing of the noise disturbers (power supplies, cooling fans, SLCOs) from the BOMPD and between them. Additionally, cable routing is optimized to eliminate the most of ground loops. Thus, despite appearance of these noise pick-ups in the phase noise error measurements (Fig. 2.7) their contribution to the overall jitter is minor.

2.4 Dual-frequency reference path

As discussed before, further suppression of the BOMPD noise floor is limited by the photodetection noise floor of the reference path of the BOMPD. Meanwhile, this limitation could be partially bypassed by decreasing of the down-mixing frequency for the modulated pulse train at the output of Sagnac-loop interferometer. This is a permissible modification while the BOMPD's maximum response frequency, which is in this case limited by the down-sampling frequency, is much higher than the PLL bandwidth.

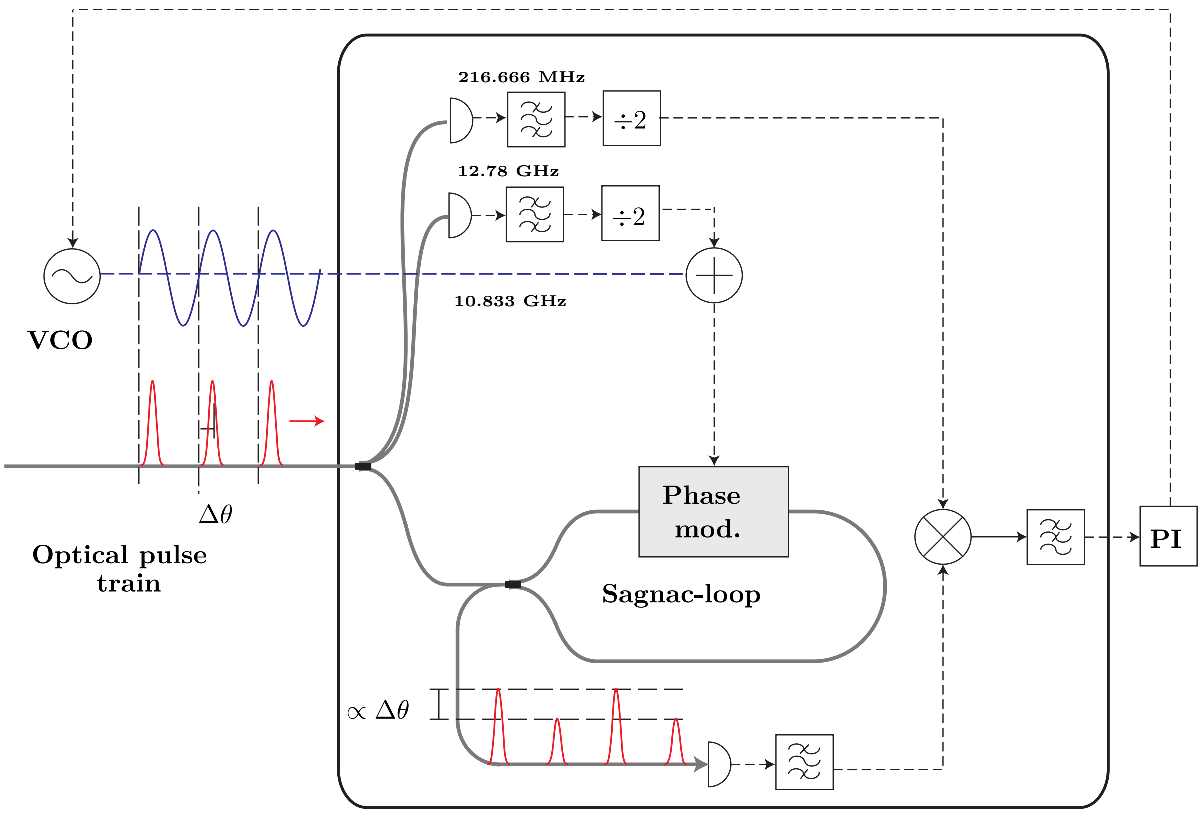

Figure 2.9: Scheme of the BOMPD with an additional independent reference path down-mixing of the modulated pulse train at the output of Sagnac-loop interferometer. Much lower operating frequency of this reference path makes possible further suppression of the photodetection noise floor without limiting of the PLL's operating bandwidth.

Additional reference path was built to perform down-conversion at 108.333 MHz which is nearly 60 times lower than the modulation frequency of 6.39 GHz. As one might expect, it is possible to increase signal-noise ratio of the directly detected optical signal by increasing of the incident optical power to +5 dBm, because of higher saturation power for lower frequencies. VCO signal was removed and the PLL unlocked to measure the noise floor of the BOMPD with the new reference paths' scheme. New modified BOMPD shows the noise floor of -161 dBc/Hz (see Fig. 2.10), which proves significant improvement of the noise performance. Sources of the parasitic pick-ups from 50 Hz to 800 Hz are discussed before. The f^{-3} low-frequency slope represents an overall impact of the noise of the detection electronics. Integrated jitter riches the value just below 0.2 fs from 1 Hz to 1 MHz Despite the fact that the low-frequency reference path was built with low-cost RF-components (Hittite, Mini-Circuits), it performs much higher resistance to temperature-induced phase shifts, since they decrease proportionally to the operating frequency.

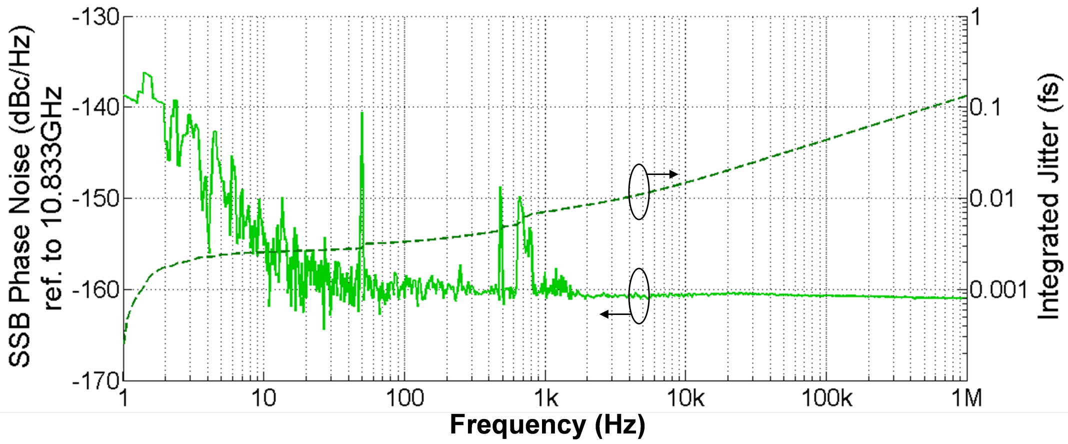

Figure 2.10: Noise floor of the BOMPD with dual-frequency reference signal detection.

3 | Interferometric setup for phase noise measurements

Development of ultra-low noise stabilization systems requires a measurement tool for characterization of their noise performance, which measurement noise floor would be even lower than than the noise floor of the stabilization system. In the case of developed BOMPDs the phase noise floor of the required measurement tool for a further research should lay below -160 dBc/Hz, referred to 10.8 GHz. In the experiments described in the previous chapter, the out-of-loop performance of the BOMPD-based PLL was directly observed by nearly identical second BOMPD with a lower noise floor. This measurement scheme shows the phase noise performance relatively to the same referencing optical signal, i.e. is not sensitive to the laser phase jitter. Alternative approach is to build two complete BOMPD-based PLLs and to measure their residual phase jitter, which will present the absolute noise performance of the stabilization system.

3.1 Setup scheme

To characterize residual phase offset between two loosely locked SLCOs, a high-precision microwave interferometric setup was built basing on research of E. N. Ivanov *et al.* [18] on corresponding techniques. The system is shown in Fig. 3.1, where the phase locked VCOs are presented as devices under test (DUT). Their output signals are balanced to have equal phase and power level with use of variable attenuators (ATM; AF066-10) and phase shifter (ATM; P1506D). Afterwards the signals are routed to the 180° hybrid coupler (MCLI; HJ-38) where they interfere constructively and destructively and could be readed out at Σ and Δ outputs, respectively. A non-zero signal at the Δ output could appear as consequence of a phase jitter of the VCO signals. This signal is amplified by the low-noise RF-amplifier (Nextec-RF; NBL00437) and then down-mixed by the carrier frequency from the Σ output. Obtained signal is then measured by spectrum analyzer. Additional RF-signal source with a slightly different from main carrier frequency is required for calibration of the interferometric system.

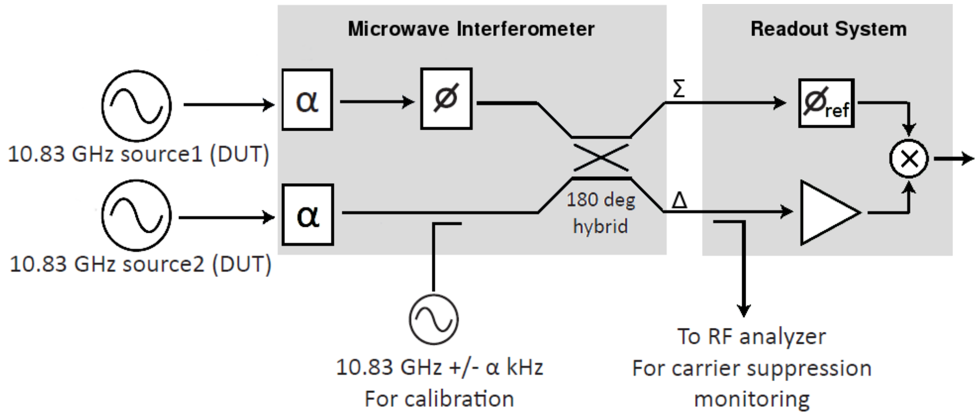

Figure 3.1: Scheme of the interferometric residual phase noise measurement system for two loosely locked microwave signal sources.

The phase noise floor of the interferometric system is mostly defined by the effective noise temperature of the readout system. This limitation for single-side spectral density comes as

$$\mathcal{L}_{\theta} = \frac{k_B T_{RS}}{P_{inp}}, \tag{3.1}$$

where $\mathcal{L}_{\theta}$ is the phase noise floor of the interferometric setup, k_B is Boltzman constant, P_{inp} is the power incident on the readout system of the setup and T_{RS} is the effective noise temperature of the readout system which presents as

$$T_{RS} = T_0 + T_{amp}, \tag{3.2}$$

where T_0 is the ambient temperature and T_{amp} is the effective noise temperature of the amplifier.

3.2 Measurement results

At first glance, the scheme of the interferometric setup could appear to be not sophisticated. However, this simplicity is compensated by the amount of laboratory electronic equipment used for calibration of the setup and essentially phase noise measurements. It is also important to note that the whole cycle of the calibration and measurement should be done with minimal mechanical and thermal disturbance of the setup. Otherwise it leads to a significant inaccuracy of the measurement results, due to overlap of amplitude modulation effects on phase noise measurement.

For test purpose, two 10.833 GHz SLCOs were loosely locked by referencing of one of these VCOs to the second one by the PI controller (NewPort; LB1005). Phase error signal was provided by to the PI-conroller by mixing of the VCO output signals in the RF-mixer (Mini-Circuits). The same 10.833 GHz signals were pre-amplified to the level of 20 dBm and routed to the inputs of the interferometric system. Precision of the amplitude and phase balancing of the input signals could estimated by a RF spectrum analyzer (Agilent; N9030A) connected to the Δ-output of the 180° coupler through the directional coupler (ATM; C116-20). Iterative tuning of the variable attenuators and phase shifter results in the suppression of the carrier frequency at the Δ-output to the level of -50 dBm. In order to obtain proper in-phase mixing in the readout system, one should tune the variable reference phase shifter and monitor the output signal by an oscilloscope. The system will be tuned correctly, if the average DC level of the output signal is equal zero. Afterwards, the output signal is switched to the spectrum analyzer (Agilent; E5052B) for the acquisition of the phase noise performance.

Obtained phase noise spectrum should be converted from voltage to radian units by calibration of the interferometric setup. Additional low-power 10.833 GHz microwave signal generator (Agilent; E8257D) with a slight frequency offset of few kHz from the main carrier is additionally driving one of the interferometer arms to artificially induce a beat note with amplitude V_{beat} in the output phase noise curve. Phase sensitivity of the readout system is then given by

$$\mathcal{K} = V_{beat} \;/\; \sqrt{\frac{P_c}{2P_{inp}}}, \tag{3.3}$$

where P_c is the power level of the calibration signal. Phase sensitivity was measured to be around 30 V/rad for the 50Ω input coupling of the measurement equipment. Scaled phase noise curve is presented in Fig. 3.2 in red.

Phase noise floor of the interferometric setup was measured by driving of the both interferometer arms with the identical 10.833 GHz signals from the single free-running SLCO. The single-sideband phase noise floor of the interferometric setup is shown in Fig. 3.2 in black. The noise floor curve reaches -185 dBc/Hz level at 10 MHz Fourier frequency. The integrated phase jitter is only 0.3 fs from 10 Hz to 100 MHz (see Fig. 3.3).

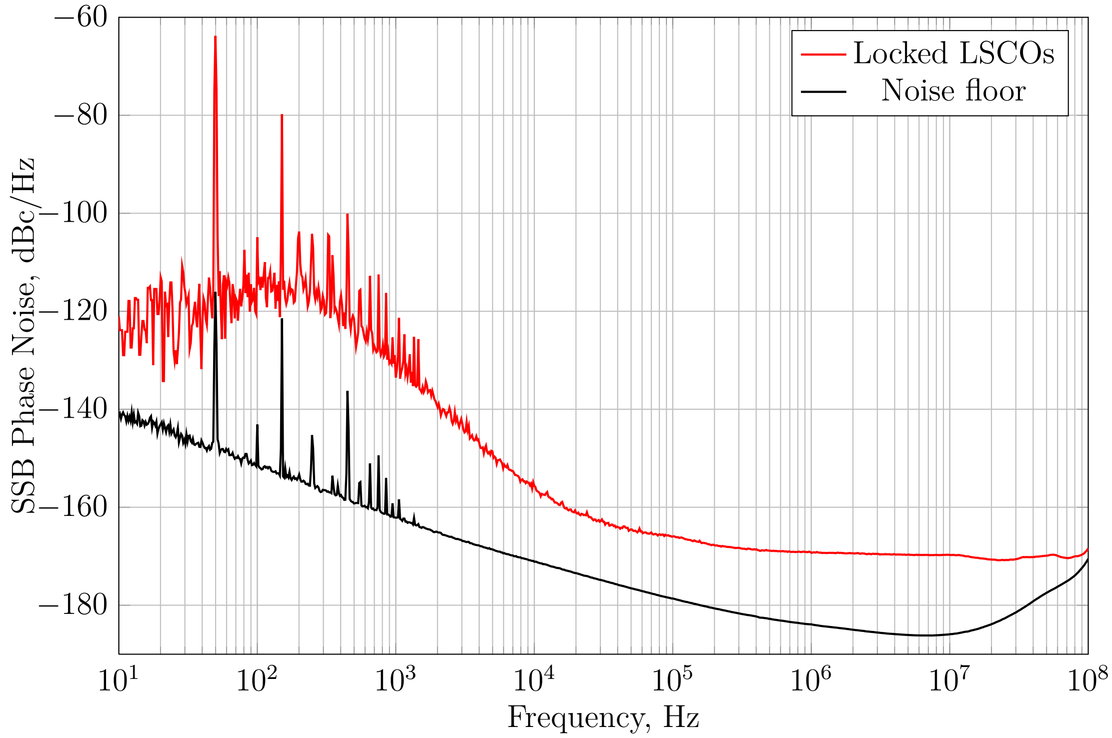

Figure 3.2: Interferometric phase error measurements for loose SLCOs locking referred to 10.833 GHz.

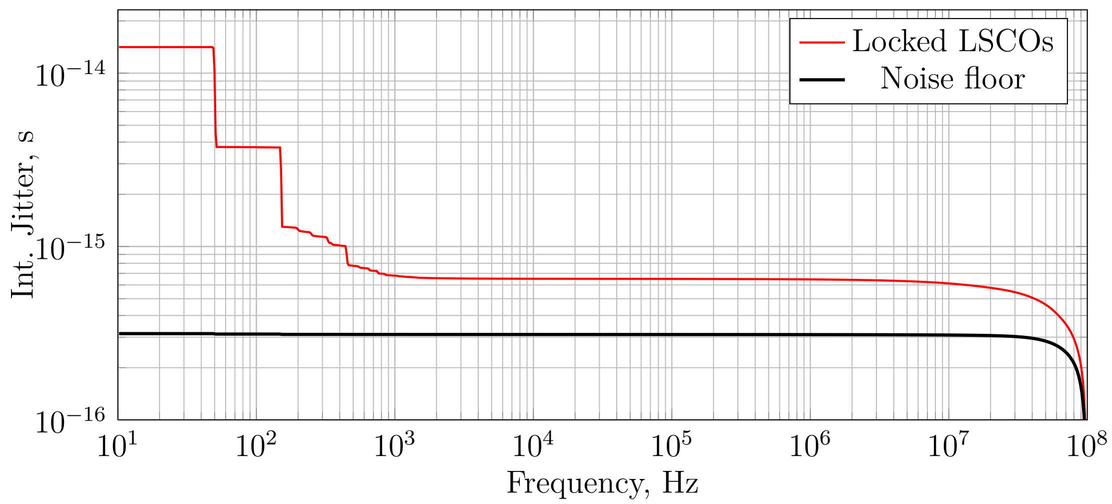

Figure 3.3: Integrated RMS timing jitter corresponding to Fig. 3.2.

4 Conclusion and outlook

The purpose of the current study was to determine the most AM-sensitive signal paths of the BOMPD by careful characterization of the noise behavior of several BOMPD configurations. RF components and optics of the system were optimized to reduce the level of noise generated within the BOMPD, relatively to its previous modifications. In the series of experiments the improved BOMPD performed referencing of RF and laser signal sources. Optical-to-RF synchronization showed only 0.5 fs RMS jitter integrated from 1 Hz to 20 kHz. Construction of the additional MHz-frequency reference path significantly suppressed the BOMPD noise floor to the level of -161 dBc/Hz. Further research might investigate increasing of the signal-noise ratio in the reference path. More elaboration is required to uncouple the BOMPD electronics from external environmental acoustical, electrical and EMI disturbers.

The assembled microwave interferometric noise measurement system showed extremely low measurement noise floor down to -185 dBc/Hz referred to 10.833 GHz carrier. This tool provides the solution for absolute phase noise characterization of the complete chain of a timing distribution system for future large-scale scientific facilities.

Acknowledgements

First of all I would like to express my gratitude to Prof. Dr. Franz X. Kärtner for giving me the opportunity to work on my thesis in the Ultrafast Optics and X-Rays Division at CFEL and its inspiring supervision. I am grateful to Dr. Ingmar Hartl for acting as second advisor for this work. Many thanks to Kwangyun Jung from Ultra-Scale Photonic Control and Measurement Group at KAIST for the very helpful knowledge exchange between our laboratories. Very special thanks go to Michael Peng from Optics and Quantum Electronics Group of RLE at MIT for sharing his experience in microwave electronics and fruitful teamwork on the BOMPD project.

A | Ultra-stable microwave VCO

In the experiments on precise phase locking of a VCO to the reference optical signal the total phase stability of the synchronization system still depends on the phase noise performance of the VCO at high-frequency offsets from the carrier, since the locking bandwidth is restricted by several MHz or less. For the investigations described in the following thesis two pieces of one of the best so far existing commercial microwave oscillators (10.833 GHz Sapphire loaded cavity oscillator from Raytheon) was used. Their phase and AM noise performance after warming up is shown in Fig. A.2. Integrated jitter of the SLCO is 2.3 fs from 100 Hz to 10 MHz and 0.3 fs from 1 kHz to 10 MHz. [15]. Output power of the output signal is +12 dBm. By default, the oscillator is working in the free-running mode. When VCO input (±10V) enabled, the generator frequency could be tuned in the range of a few kHz. Additional slow tuning of the frequency could be done manually (±200 kHz) and by driving of the VCF input (few hundred kHz) with time constant about 30 s.

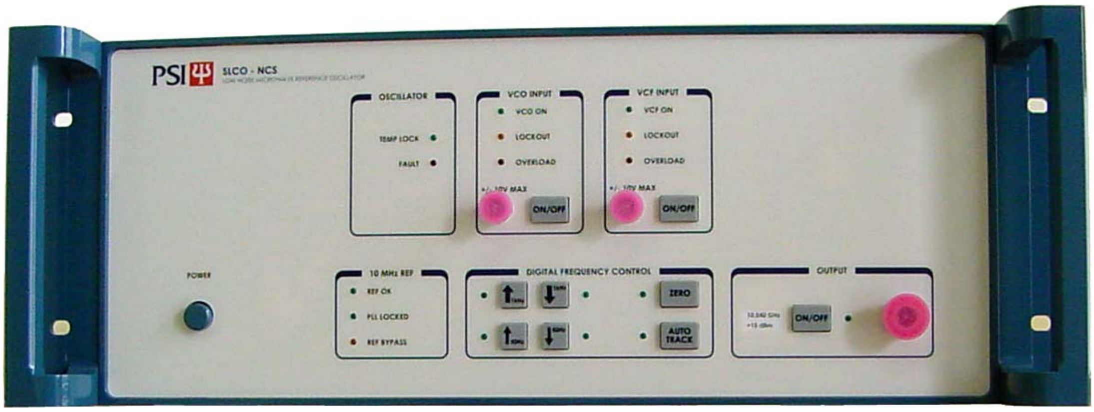

Figure A.1: Front panel of the SLCO mounted in a 19-inch utility rack.

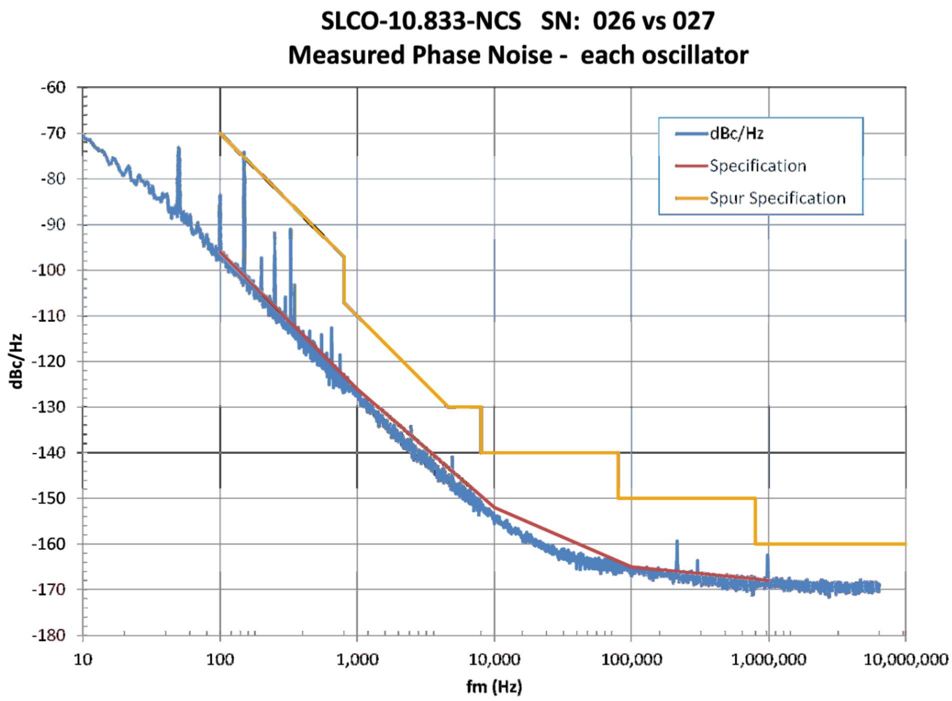

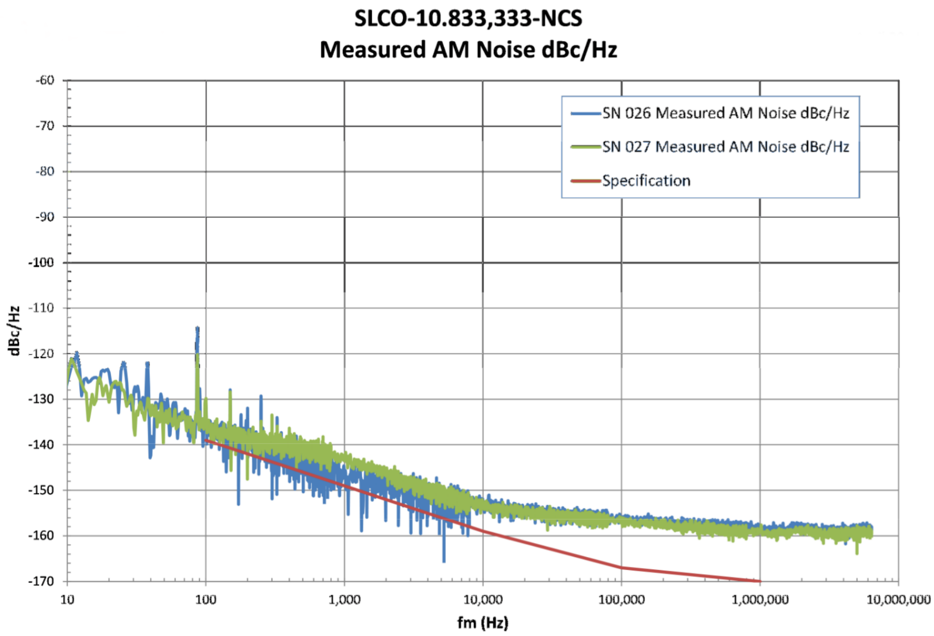

Figure A.2: Variation of the single-sideband (SSB) phase noise (*top*) and AM noise (*bottom*) performance of free-running SLCOs at 10.833 GHz carrier frequency with offset from carrier frequency.

B | Low-noise amplifier

A low-noise preamp with a fixed linear gain was required to amplify the error signals above the measurement noise floor. OPA847 operational amplifier was chosen as a proper low-cost solution for the described issue. The circuit of the amplifier with gain 100 is shown in Fig. B.1. Measured frequency response of the preamp (see Fig.B.2) shows linearity of the gain up to MHz frequencies.

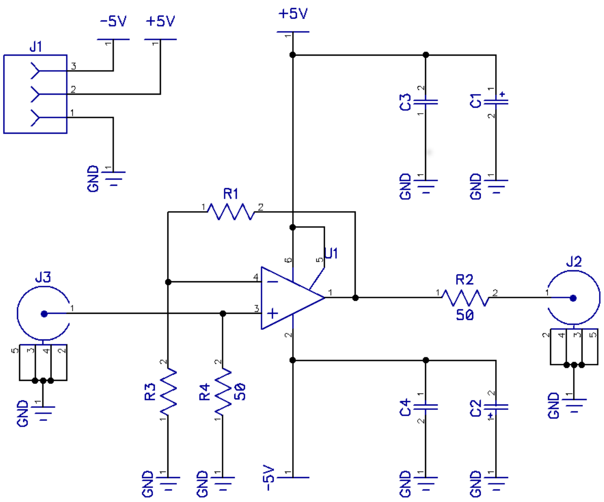

RefDes	Value
C1	6.8uF
C2	6.8uF
C3	0.1uF
C4	0.1uF
J1	FCI-20020111
J2	SMA 132289
J3	SMA 132289
R1	5k
R2	50
R3	50
R4	50
U1	OPA847

Figure B.1: Preamplifier's electrical circuit and BOM.

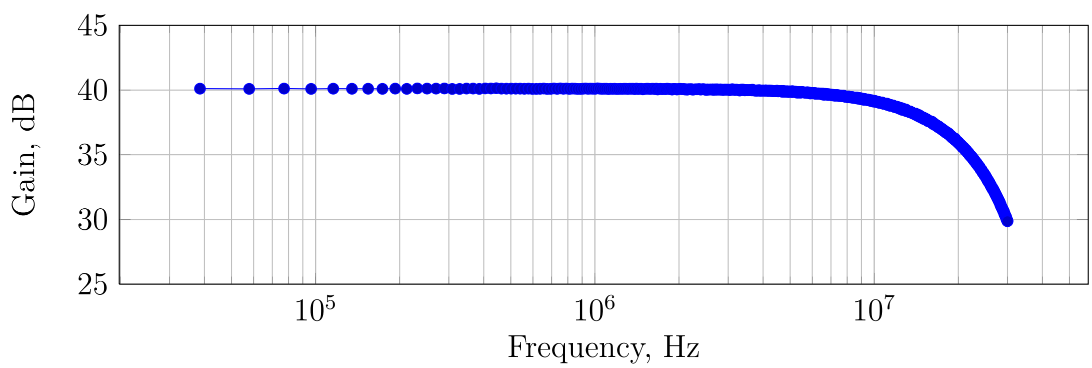

Figure B.2: Frequency response of the amplifier.

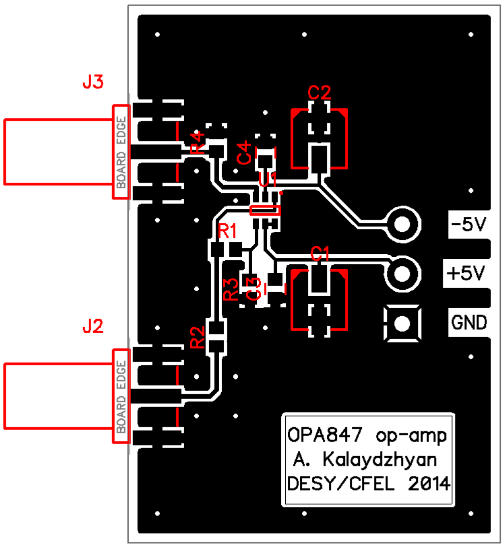

Figure B.3: Top side of the amplifier's PCB

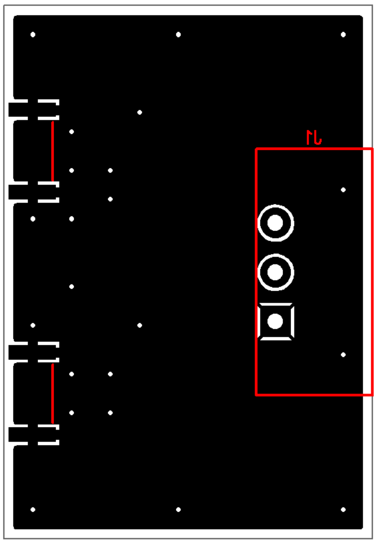

Figure B.4: Bottom side

The amplifier was assembled on the designed double layer PCB, which layout is shown on Fig. B.3 and B.4. After placing of the PCB into the aluminum case the value of the output shot noise of the amplifier have settled on -71dBm (see Fig.B.5).

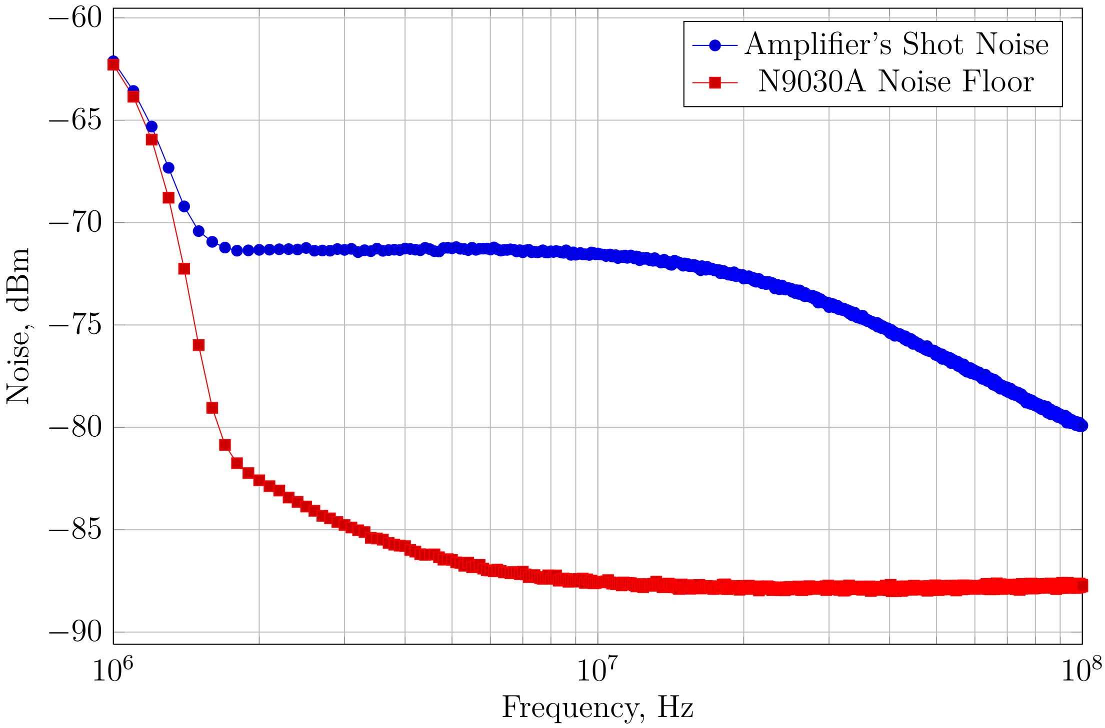

Figure B.5: Bottom side of the amplifier's PCB

C | Calibration of the BOMPD setup

Phase noise performance of a BOMPD-based PLL captured by the spectrum analyzer required to be transformed from voltage to radian units. In order to measure the BOMPD phase error sensitivity one should manually tune the VCO close to the reference frequency without locking of the PLL. Afterwards, BOMPD's output signal should be routed to an oscilloscope. Example of the scope picture captured by the oscilloscope is shown in Fig. C.1. Due to the non-zero error frequency between the VCO and reference pulses their phase offset is continuously growing. Thus, output signal cyclic repeats the form of the Sagnac-interferometer transmission function. Maximum sensitivity is reached when the equilibrium level for the loop filter is settled to the highest slope of the curve. According to the fact that the Sagnac-interferometer transmission function covers 2π phase offset between its maximums, calibration constant of the BOMPD is given by

$$\mathcal{K}_{BOMPD} = 2\pi f / \frac{\Delta V}{\Delta \tau}, \tag{C.1}$$

where ΔV and $\Delta \tau$ are the slope dimensions and $1/f$ is the time interval between two maximums of the captured signal.

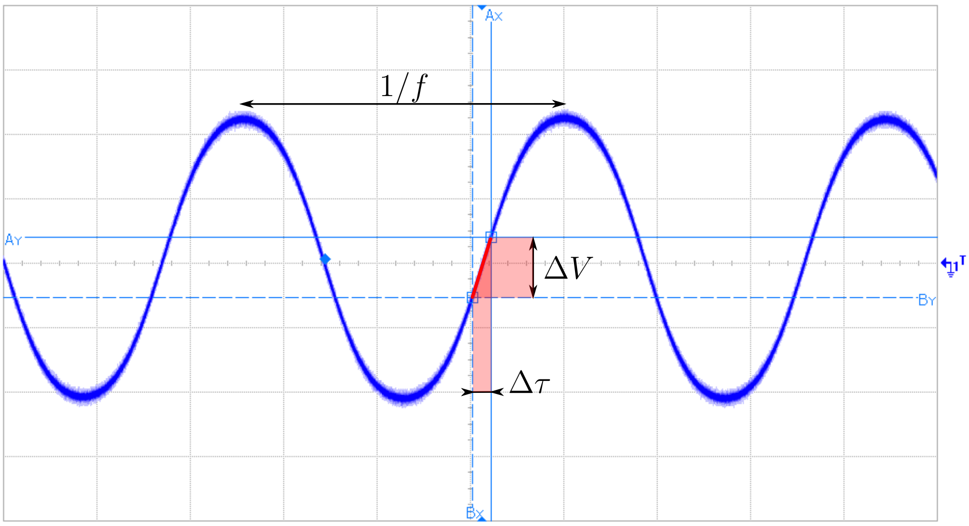

Figure C.1: Example of the BOMPD output signal when locking is switched off.

References

[1] R. S. A. of Sciences, "The nobel prize in physics 2005." Online; 6 Oct 2014: `http://www.nobelprize.org/nobel_prizes/physics/laureates/2005/`.

[2] T. J. Kippenberg, R. Holzwarth, and S. A. Diddams, "Microresonator-based optical frequency combs," *Science*, vol. 332, no. 6029, pp. 555–559, 2011.

[3] R. Ell, U. Morgner, F. X. Kärtner, J. G. Fujimoto, E. P. Ippen, V. Scheuer, G. Angelow, T. Tschudi, M. J. Lederer, A. Boiko, and B. Luther-Davies, "Generation of 5-fs pulses and octave-spanning spectra directly from a ti:sapphire laser," *Opt. Lett.*, vol. 26, no. 6, pp. 373–375, 2001.

[4] A. Benedick, "Applications and Noise Properties of High Repetition Rate Titanium: Sapphire Frequency Combs," *Dissertation Abstracts International*, 2011.

[5] K. Holman, R. Jones, A. Marian, S. Cundiff, and J. Ye, "Detailed studies and control of intensity-related dynamics of femtosecond frequency combs from mode-locked ti:sapphire lasers," *Selected Topics in Quantum Electronics, IEEE Journal of*, vol. 9, pp. 1018–1024, July 2003.

[6] L. Matos, O. D. Mücke, J. Chen, and F. X. Kärtner, "Carrier-envelope phase dynamics and noise analysis in octave-spanning ti:sapphire lasers," *Opt. Express*, vol. 14, no. 6, pp. 2497–2511, 2006.

[7] D. C. Heinecke, A. Bartels, and S. A. Diddams, "Offset frequency dynamics and phase noise properties of a self-referenced 10 ghz ti:sapphire frequency comb," *Opt. Express*, vol. 19, no. 19, pp. 18440–18451, 2011.

[8] Zwart et al., "The MIT Bates X-Ray Laser Project," in *Proceedings of PAC*, (Portland), 2003.

[9] Abela et al., *XFEL: The European X-Ray Free-Electron Laser - Technical Design Report.* Hamburg: DESY, 2006.

[10] M. Y. Peng, P. T. Callahan, A. H. Nejadmalayeri, S. Valente, M. Xin, L. Grüner-Nielsen, E. M. Monberg, M. Yan, J. M. Fini, and F. X. Kärtner, "Long-term stable,

sub-femtosecond timing distribution via a 1.2-km polarization-maintaining fiber link: approaching 10^{-21} link stability," *Opt. Express*, vol. 21, no. 17, pp. 19982–19989, 2013.

[11] A. Winter, *Fiber Laser Master Oscillators for Optical Synchronization Systems.* PhD thesis, 2008.

[12] B. Lorbeer, J. Mueller, F. Ludwig, F. Loehl, H. Schlarb, and A. Winter, "Noise and drift characterization of critical components for the laser based synchronization system at flash," in *Proceedings of DIPAC 2007*, (Venice, Italy), 2007.

[13] X. Xie, Q. Zhou, K. Li, A. Beling, and J. C. Campbell, "1.8 Watt RF Power and 60% Power Conversion Efficiency Based on Photodiode Flip-chip-bonded on Diamond," in *Conference on Lasers & Electro-Optics, Optical Society of America*, p. JTh5B.9, 2014.

[14] T. M. Fortier, F. Quinlan, A. Hati, C. Nelson, J. A. Taylor, Y. Fu, J. Campbell, and S. A. Diddams, "Photonic microwave generation with high-power photodiodes," *Opt. Lett.*, vol. 38, no. 10, 2013.

[15] "Report on performance of SLCO-10.833,333-NCS," tech. rep., Raytheon Australia, 2013.

[16] J. Kim, F. X. Kärtner, and M. H. Perrott, "Femtosecond synchronization of radio frequency signals with optical pulse trains," *Optics letters*, vol. 29, pp. 2076–8, Sept. 2004.

[17] J. Kim, *High-Precision Optical and Microwave Signal Synthesis and Distribution.* PhD thesis, 2007.

[18] E. Ivanov, M. Tobar, and R. Woode, "Microwave interferometry: application to precision measurements and noise reduction techniques," *Ultrasonics, Ferroelectrics, and Frequency Control, IEEE Transactions on*, vol. 45, pp. 1526–1536, Nov 1998.